# $^{18}$F-DCFPyL PET/CT in Patients with Subclinical Recurrence of Prostate Cancer: Effect of Lesion Size, Smoothing Filter, and Partial-Volume Correction on PROMISE Criteria

Claudia Ortega*[1], Josh Schaefferkoetter*[1,2], Patrick Veit-Haibach[1], Reut Anconina[1], Alejandro Berlin[3], Nathan Perlis[4], and Ur Metser[1]

[1]*Joint Department of Medical Imaging, Princess Margaret Hospital, University Health Network, Mount Sinai Hospital and Women's College Hospital, University of Toronto, Toronto, Ontario, Canada;* [2]*Siemens Healthcare Limited, Oakville, Ontario, Canada;* [3]*Radiation Medicine Program, Princess Margaret Hospital, University Health Network, Toronto, Ontario, Canada; and* [4]*Urologic Oncology, University Health Network, Princess Margaret Cancer Centre Research Institute, University of Toronto, Toronto, Ontario, Canada*

Our purpose was to determine the effect of a smoothing filter and partial-volume correction (PVC) on measured prostate-specific membrane antigen (PSMA) activity in small metastatic lesions and to determine the impact of these changes on molecular imaging PSMA (miPSMA) scoring. **Methods:** Men who had biochemical recurrence of prostate cancer with negative findings on CT and bone scintigraphy were referred for $^{18}$F-DCFPyL (2-(3-(1-carboxy-5-[(6-$^{18}$F-fluoro-pyridine-3-carbonyl)-amino]-pentyl) PET/CT. Examinations were performed on 1 of 2 different brands of PET/CT scanner. All suspected tumor sites were manually contoured on coregistered CT and PET images, and each was assigned an miPSMA score as per the PROMISE criteria. The PVC factors were calculated for every lesion using the anatomic CT and then applied to the unsmoothed PET images. The miPSMA scores, with and without the corrections, were compared, and a simplified rule-of-thumb (RoT) correction factor (CF) was derived for lesions at various sizes (<4 mm, 4–7 mm, 7–9 mm, and 9–12 mm). This CF was then applied to the original dataset and the miPSMA scores that were obtained using the RoT CF were compared with those obtained using the actual corrections. **Results:** There were 75 men (median age, 69 y; median serum PSA, 3.69 μg/L) with 232 metastatic nodes less than 12 mm in diameter (mean lesion volume, 313.5 ± 309.6 mm$^3$). The mean $SUV_{max}$ before and after correction was 11.0 ± 9.3 and 28.5 ± 22.8, respectively ($P < 0.00001$). The mean CF for lesions smaller than 4 mm ($n = 22$), 4–7 mm ($n = 140$), 7–9 mm ($n = 50$), and 9–12 mm ($n = 20$) was 4 (range, 2.5–6.4), 2.8 (range, 1.6–4.9), 2.3 (range, 1.6–3.3), and 1.8 (range, 1.4–2.4), respectively. Overall, the miPSMA scores were concordant between the corrected dataset and the RoT dataset for 205 of 232 lesions (88.4%). **Conclusion:** A smoothing filter and PVC had a significant effect on measured PSMA activity in small nodal metastases, impacting the miPSMA score.

**Key Words:** genitourinary; PET/CT; PSMA; partial-volume correction; prostate cancer; subclinical

**J Nucl Med 2020; 61:1615–1620**
DOI: 10.2967/jnumed.120.241737

Prostate-specific membrane antigen (PSMA) PET imaging offers unparalleled accuracy in the assessment of patients with prostate cancer. The main evaluated clinical indications to date for PSMA PET are for restaging of patients with prostate cancer after primary therapy with biochemical failure or for the initial staging of high-risk or unfavorable intermediate-risk prostate cancer (*1*). Various PSMA tracers are available. The most widely used PSMA radiotracer is $^{68}$Ga-PSMA-11 (also named $^{68}$Ga-PSMA-HBED-CC). Recently introduced $^{18}$F-labeled PSMA tracers have the advantage of cyclotron production, enabling multiple doses from a single formulation. In addition, $^{18}$F has a longer half-life than $^{68}$Ga, facilitating shipping of the tracer to off-site facilities, and the lower energy and shorter positron range allow for higher image resolution (*2*). One such tracer is $^{18}$F-DCFPyL (2-(3-(1-carboxy-5-[(6-$^{18}$F-fluoro-pyridine-3-carbonyl)-amino]-pentyl), a promising second-generation low-molecular-weight ligand (*3*).

Recently, the Prostate Cancer Molecular Imaging Standardized Evaluation (PROMISE) criteria were introduced to standardize the interpretation of PSMA PET images (*4*). PROMISE suggests a molecular imaging TNM system (miTNM, version 1.0). In this staging algorithm, each suspected primary or recurrent tumor (T), regional nodal metastasis (N), and distant metastasis (M1a–M1c) is assigned a diagnosis of positive, negative, or equivocal depending on the degree of PSMA expression and the findings on morphologic imaging (CT or MRI). PSMA PET uptake at suspected tumor sites is quantified using a PSMA scoring system relative to the physiologic uptake in reference tissues, with the parotid gland, liver, and blood-pool activity serving as the reference for high, intermediate, and low PSMA uptake, respectively (Table 1).

For accurate quantification of radiotracer uptake on PET, several corrections are needed, such as taking the partial-volume effect into account (*5*). The partial-volume effect originates from the finite spatial resolution of the PET scanner and causes an

Received Jan. 6, 2020; revision accepted Mar. 9, 2020.
For correspondence or reprints contact: Ur Metser, Department of Medical Imaging, University of Toronto, Joint Department of Medical Imaging, 610 University Ave., Suite 3-960, Toronto, Ontario, Canada M5G 2M9.
E-mail: ur.metser@uhn.ca
*Contributed equally to this work.
Published online Mar. 20, 2020.

**TABLE 1**
PSMA Scoring System

| Score | PSMA expression | Uptake |
|---|---|---|
| 0 | None | <Blood-pool activity |
| 1 | Low | ≥Blood pool and <liver |
| 2 | Intermediate | ≥Liver and <parotid gland |
| 3 | High | ≥Parotid gland |

**TABLE 2**
Original Versus Corrected Parameters for All Lesions

| Parameter | Original | Corrected |
|---|---|---|
| Mean $SUV_{max}$ ($P < 0.00001$) | 11.0 ± 9.3 (1.8–57.1) | 28.5 ± 22.8 (5.1–116.3) |
| Mean $SUV_{mean}$ ($P < 0.00001$) | 6.7 ± 5.7 (1–36.3) | 14.1 ± 11.3 (2.2–54.8) |
| Mean miPSMA score ($P < 0.00001$) | 1.6 ± 0.76 (1–3) | 2.28 ± 0.77 (1–3) |

Data are mean ± SD, followed by range in parentheses.

underestimation of the measured activity concentration, especially for lesions at or below the resolution of the scanner (*6*). The partial-volume effect in medical imaging results from the combination of limited scanner resolution and heterogeneous tissue types within voxels of finite dimensions. Accurate quantification of metabolic volumes when they are below 2 or 3 times the spatial resolution of the PET scanner is hampered by the partial-volume effect, leading to underestimation of SUV or even underdetection of small lesions (*7*). Furthermore, PET images are affected by routinely applied gaussian filters. These effects degrade resolution and quantitative accuracy and are especially problematic for PET imaging because of its relatively coarse pixel sizes.

Two factors—a smoothing filter and partial-volume correction (PVC)—may play a significant role in the measured individual lesion activity, particularly for small-volume tumor foci. These are increasingly common as PSMA PET is adopted for the management of prostate cancer, especially in patients with subclinical recurrent or metastatic disease, with no gross detectable metastatic disease on CT or bone scintigraphy. In these patients, accurate identification of all disease sites may have significant clinical implications in tailoring the most appropriate therapeutic approach. The aim of the current study was to determine and quantify the effect of a smoothing filter and PVC on measured PSMA activity in small metastatic lesions (e.g., <12 mm) and to ascertain their impact on molecular imaging PSMA (miPSMA) scoring.

## MATERIALS AND METHODS

### Patient Population

The cohort for this study included patients from 2 prospective institutional ethics review board–approved clinical trials from May 2018 to February 2019 (NCT03718260 and NCT03160794). Written informed consent was obtained from all subjects. In both trials, subjects who had completed primary therapy experienced biochemical recurrence with subclinical metastasis, which was defined as asymptomatic recurrence with negative or equivocal findings on conventional imaging (bone scintigraphy and CT). CT and bone scintigraphy were interpreted clinically before study accrual. Patients underwent $^{18}$F-DCFPyL PET/CT between May 2018 and February 2019.

### $^{18}$F-DCFPyL PET Imaging

$^{18}$F-DCFPyL was synthesized as previously described (*8*). PET was performed on 1 of 2 scanners (mCT40 [Siemens Healthcare] or Discovery 610 [GE Healthcare]) approximately 120 min (mean, 115.1 min; range, 83–168 min) after intravenous injection of 335.5 MBq (range, 223–376 MBq) of $^{18}$F-DCFPyL, a second-generation low-molecular-weight PSMA PET radiotracer. The patients were asked to void the bladder and were subsequently positioned supine on the imaging couch with the arms outside the region of interest. Images were obtained from the top of the skull to the upper thighs. Iodinated oral contrast material was administered for bowel opacification; no intravenous iodinated contrast material was used. The acquisition time was 8 min per bed position for the pelvis and 2 min per bed position for all other sites. Overall, 5–9 bed positions were obtained, depending on patient height. For the mCT40, the CT parameters were 120 kV, a 5.0-mm slice width, a 4.0-mm collimation, a 0.8-s rotation time, an 8.4-mm feed per rotation, and a B30s kernel medium smoothing reconstruction. A PET emission scan using time of flight with scatter correction was obtained covering the identical transverse field of view, with a 2.6-pixel image size, a 3.27-mm slice width, and a gaussian filter of 5 mm in full width at half maximum with 31 iterations and 21 subsets. For the Discovery 610, the CT parameters were 120 kV, 150–190 mA depending on body weight, a 3.75-mm helical thickness, an 0.8-s rotation time, an 11.25-mm feed per rotation, and standard reconstruction at a 2.5-mm slice width. The PET parameters were a 3.18-pixel image size and a gaussian filter of 6.4 mm in full width at half maximum with 2 iterations and 32 subsets. The scanning parameters were the clinical standard at each site and were selected according to vendor recommendations for each scanner.

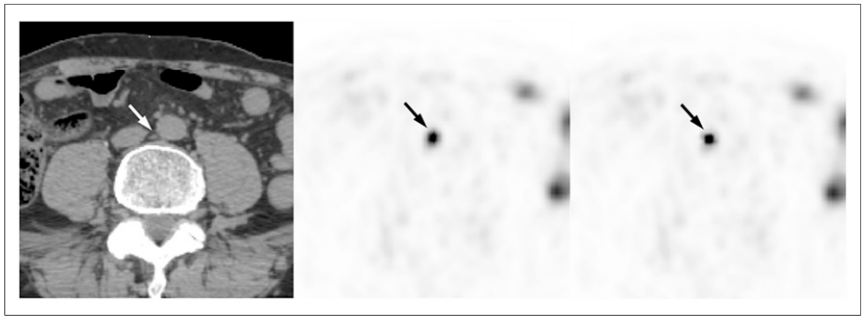

**FIGURE 1.** A 75-y-old man with history of pT3a Gleason 7 (3 + 4) prostate cancer after radical prostatectomy 11 y ago, and salvage radiotherapy for biochemical recurrence 7 y ago, now with slowly rising PSA (2.1 ng/mL). Interaortocaval lymph node (left panel, arrow) had volume of 118.3 $cm^3$ on CT. $SUV_{max}$ measured on PET was 7.0 with miPSMA score of 1 (middle panel, arrow). After correction, $SUV_{max}$ was 22.6 with miPSMA score of 3 (right panel, arrow).

### Image Analysis

All suspected tumor foci on $^{18}$F-DCFPyL PET/CT were manually contoured on the unenhanced CT images (acquired at the time of PET/CT) and, independently, on the 5-mm gaussian-smoothed PET images, using a Mirada Vision workstation (Mirada Medical). Two readers worked together in consensus, one performing the contouring and the other reviewing it. For all lesions, $SUV_{max}$ and $SUV_{mean}$ were recorded.

A threshold of 41% of $SUV_{max}$ was used to generate a contoured volume ($mm^3$). This threshold was used because it has been previously suggested to represent the optimal volume match (*9*). For a reference, the $SUV_{max}$ and $SUV_{mean}$ of the right parotid gland, liver (as measured over the right hepatic lobe), and mediastinal blood pool were recorded. Each lesion received a miPSMA score (before the correction was performed) as per the PROMISE criteria.

### Correction Methodology

For all analyses in this work, unsmoothed PET image data were used. Because the data were collated retrospectively from a cohort of patients in ongoing clinical trials, postreconstruction smoothing had already been applied to the images. The unsmoothed data were obtained by Richardson–Lucy deconvolution (*10,11*). We validated this method within a subset of patients having available PET raw data, which were directly reconstructed without a smoothing filter for comparison.

CT and PET mask volumes were generated from the contours using slice-by-slice selection of the pixels contained within the region contour points. To account for local alignment inconsistencies between PET and CT images, for each lesion in the CT data we found translational offsets that maximized the region-of-interest $SUV_{peak}$ within the activity in the PET volume delineated by the corresponding region in the PET mask. The CT mask was then transformed to the PET space by linear interpolation onto the PET voxel coordinate grid, accounting for any necessary translational adjustments. Lesion volume and SUV data were recorded from the contoured lesions (i.e., the original dataset).

The matched anatomic mask was the basis for calculating the PVC factors. However, before the corrections factors could be calculated, the relative contrast for each node needed to be represented in the mask, since local differences between region and background values determine partial-volume spill-over effects. This step was accomplished through an empiric searching approach; every region was scaled by a large range of contrast values, each time followed by calculation of its respective PVC map. The correction maps were then applied to the PET volumes, and the resulting corrected activity distributions were summed over all affected voxels. The points of the sum data were fit to a curve, and the location on the curve that equaled the corresponding sum of the original data indicated that the total mass of activity had been preserved and hence yielded the correct scaling factor. The method outlined here describes an approach for PVC for lymph nodes in PET images, with the assumption of uniformly distributed activity within small volumes.

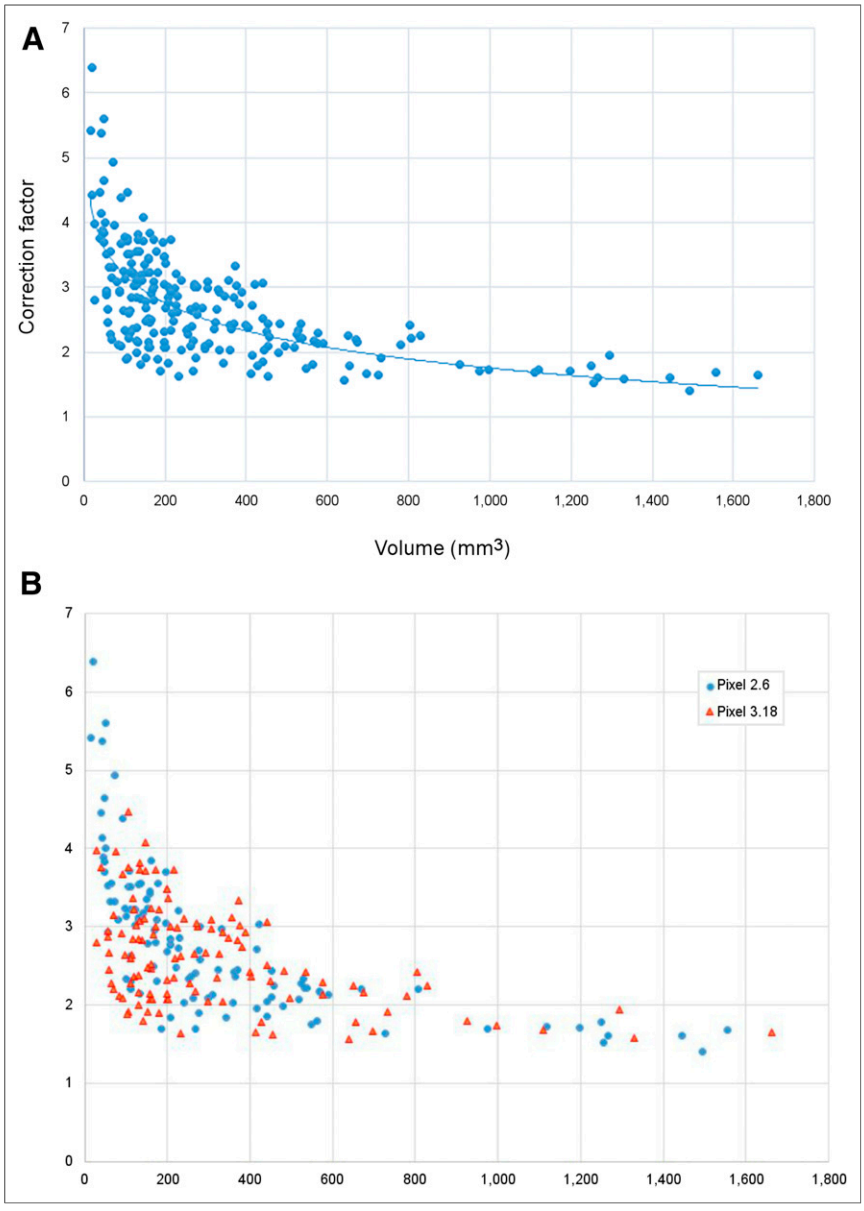


**FIGURE 2.** CF per lesion volume. (A) Distribution of CFs (*y*-axis) is graphed by lesion volume in $mm^3$ (*x*-axis). (B) CF is graphed by volume and pixel size.

Once each region of interest in the mask was corrected and scaled appropriately against a unitary background, a map of the local PVC factors was generated. Partial-volume effects were first simulated in the anatomic mask by filtering the volume by a 3-dimensional smoothing kernel consistent with the intrinsic scanner response function (in this experiment, a gaussian kernel of 4 mm in full width at half maximum was used to model the point-spread response). Dividing the original anatomic volume by the smoothed data yielded a map of correction factors (CFs), which were then applied directly to the PET volume.

The effects of the PVC were evaluated for all regions in both unsmoothed and 5-mm gaussian smoothed images. The original versus corrected $SUV_{max}$ and $SUV_{mean}$ were compared.

Subsequently, the prospectively assigned miPSMA score was compared with the score obtained from the corrected dataset (Fig. 1). All quantitative and qualitative assessments were correlated for lesion volume. Furthermore, a CF was calculated as follows: [$SUV_{max}$ with PVC correction]/[original $SUV_{max}$] for each lesion. To determine whether differences in pixel sizes from the 2 scanners have a significant impact on PVC method, the datasets were also analyzed separately for each scanner.

**TABLE 3**
CF per Lesion Size

| Lesion size | CF |
|---|---|
| <4 mm ($n$ = 22) | 4 (2.5–6.4 ± 1.1) |
| 4–7 mm ($n$ = 140) | 2.8 (1.6–4.9 ± 0.64) |
| 7–9 mm ($n$ = 50) | 2.3 (1.6–3.3 ± 0.43) |
| 9–12 mm ($n$ = 20) | 1.8 (1.4–2.4 ± 0.64) |

Data are mean followed by range ± SD in parentheses.

Because, in routine clinical work, it is not practical to contour each node, the mean CF for lesions according to size groups was calculated. The size groups chosen were nodes larger than 9 mm along the short axis (considered abnormal on morphologic imaging), nodes smaller than 4 mm (within range of scanner spatial resolution), and 2 categories for nodes between 4 and 9 mm (4–7 mm and 7–9 mm). This step was done to generate a rule-of-thumb (RoT) CF according to lesion size that could be used clinically. As a validation, the adjusted dataset using the mean CF per lesion size group was compared with the corrected SUV dataset. Similarly, the miPSMA scores were adjusted using unsmoothed reference tissues and were compared with the corrected dataset following the same methodology.

### Statistical Analysis

Statistical analysis was performed using Past software, version 3.26. Paired Student $t$ testing was used to compare lesion $SUV_{max}$ before and after corrections for the entire cohort and for each lesion size group. PSMA scores before and after corrections were compared for each size group using $\chi^2$ testing. A $P$ value of 0.05 or less was deemed statistically significant.

## RESULTS

In total, 142 men who had biochemical recurrence of prostate cancer with negative CT and bone scintigraphy findings were referred for $^{18}$F-DCFPyL PET/CT. Of these, 67 patients were excluded from analysis because of negative PET findings ($n$ = 52), lesions that could not be reliably contoured ($n$ = 13), and indeterminate lung nodules ($n$ = 2). The final study cohort consisted of 75 men with a median age of 69 y (range, 50–89 y) who had undergone radical prostatectomy ($n$ = 69), brachytherapy ($n$ = 5), or focal ablation therapy with high-intensity focused ultrasound ($n$ = 1). Median serum PSA was 3.69 μg/L (range, 0.55–49.9 μg/L).

Overall, there were 271 suspected metastases on $^{18}$F-DCFPyL PET/CT. Of them, 39 lesions were excluded because of an inability to accurately contour them on the unenhanced CT ($n$ = 29) or PET ($n$ = 10) images. For example, bone lesions visualized on PET could not be contoured because of the absence of a morphologic correlate on CT, or delineation was difficult on PET because lesions were adjacent to structures with high physiologic PSMA activity such as the ureter or bladder. The final cohort consisted of 232 well-defined nodal deposits (111 for the mCT40 and 121 for the Discovery 610).

### Original Versus Corrected Lesion Parameters

The mean lesion volume was 313.5 ± 309.6 $mm^3$ (range, 15.3–1,661 $mm^3$). Comparison of $SUV_{max}$, $SUV_{mean}$, and miPSMA score before and after correction is described in Table 2. The CF as a function of lesion volume and pixel size for the 2 different scanners is displayed in Figures 2A and 2B. The mean CF by size group is provided in Table 3. The differences between the original or corrected $SUV_{max}$ and the corresponding miPSMA score are presented as a function of lesion size in Table 4 and Figure 3. The corrected and RoT $SUV_{max}$ and miPSMA scores are shown in Table 5, and the distribution of miPSMA scores per lesion size for the various groups is in Table 6.

### Corrected Versus RoT Lesion Parameters

The $SUV_{max}$ and miPSMA scores obtained before and after correction and using the RoT CF are presented in Table 3. Overall, the miPSMA scores were concordant between the corrected dataset and the RoT dataset for 205 of 232 lesions (88.4%). The level of concordance was moderate for small lesions and increased with lesion size (68.2% [15/22] for lesions < 4 mm in diameter, increasing to 90.5% [190/210] for lesions > 4 mm in diameter).

## DISCUSSION

The recently introduced PROMISE criteria are a standardized reporting framework for PSMA-ligand PET. Functional data from PET, including degree of tracer uptake compared with physiologic uptake in reference tissues, are used in conjunction with morphologic imaging data and clinical likelihood to derive a probability of malignancy. Local tumor extent, nodal metastases, and distant metastases are assigned a molecular imaging TNM (miTNM) category. Although for regional nodes any PSMA uptake is considered positive for metastases, for nodes in less common locations for metastases, namely those outside the abdomen or pelvis, the degree of PSMA uptake impacts interpretation. For example, a supraclavicular lymph node with an miPSMA score of 1 would be

**TABLE 4**
Original Versus Corrected $SUV_{max}$ and miPSMA Scores

| | Original | | Corrected | |
|---|---|---|---|---|
| Lesion size | $SUV_{max}$ | miPSMA | $SUV_{max}$ | miPSMA |
| <4 mm | 5.3 ± 5.2 (2.1–25.6) | 1.1 ± 0.5 | 21.5 ± 21.2 (5.6–96.3), $P$ = 0.00072 | 2.1 ± 0.8, $P$ < 0.00001 |
| 4–7 mm | 8.4 ± 6.0 (1.8–34.3) | 1.4 ± 0.6 | 24.4 ± 19.7 (5.1–116.3), $P$ < 0.00001 | 2.2 ± 0.8, $P$ < 0.00001 |
| 7–9 mm | 16.4 ± 9.2 (3.7–45.8) | 2.0 ± 0.8 | 39.0 ± 25.5 (5.8–102.9), $P$ < 0.00001 | 2.6 ± 0.7, $P$ < 0.00001 |
| 9–12 mm | 22.2 ± 15.6 (3.8–57.1) | 2.2 ± 0.9 | 39.2 ± 27.1 (8.4–102.0), $P$ = 0.00004 | 2.5 ± 0.8, $P$ = 0.114 |

Data are mean ± SD with or without range in parentheses. $P$ values are for original vs. corrected data.

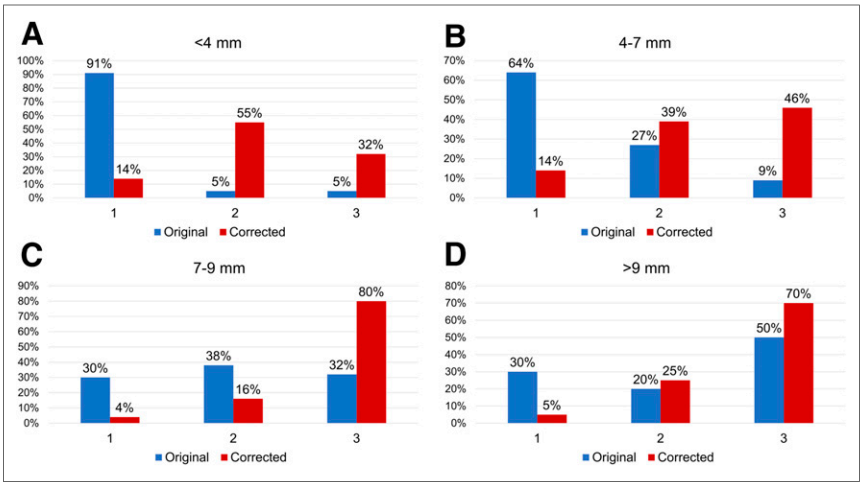


**FIGURE 3.** Distribution of PSMA scores as function of lesion size before and after smoothing filter and PVC for lesions below 4 mm (A), between 4 and 7 mm (B), between 7 and 9 mm (C), and between 9 and 12 mm (D).

considered negative, whereas if avidity is above liver uptake (miPSMA score of 2), the node would be considered positive for metastatic disease.

The role of PSMA PET in identifying patients with oligometastatic prostate cancer likely to benefit from metastasis-directed ablative therapies is evolving. This therapeutic approach aims to obtain disease control by treating all molecularly unveiled disease foci, thereby delaying or potentially avoiding the need for systemic therapies (*12–14*). PSMA PET is increasingly being used earlier during prostate cancer staging and restaging, when conventional morphologic imaging (e.g., CT and bone scintigraphy) shows negative results, highlighting the importance of these corrections for adequate characterization of subclinical small-volume metastases.

In this work, we have shown that postreconstruction smoothing and PVC have a significant effect on quantitative and qualitative characterization of small nodal deposits. PSMA score may be sensitive to small variations in pixel SUV; therefore, quantitative accuracy is an important consideration for reliable and reproducible interpretation. The effect of image smoothing and PVC on semiquantitative uptake values for small lymph nodes on PSMA PET, as expressed by the calculated CF, decreases exponentially with lesion size. As a result, the influence of this correction on the miPSMA score assigned to each lesion is greater for smaller lesions. For all lesions at least 7 mm in diameter, an miPSMA score of 1 was assigned to 110 of 162 (68%) lesions, compared with 36 of 162 (22.2%) after correction. Although there is a higher signal recovery for small lesions with a smaller pixel size (Fig. 2A), the overall trend was similar for both pixel-size images evaluated in this study.

These correction methods are time-consuming and technically challenging and are impractical for routine adoption in clinical practice. Nonetheless, quantitative accuracy is becoming increasingly important in precision cancer imaging for clinical diagnosis (improving consistency across multicenter clinical trials) and for therapy planning and delivery (*15*). As such, we suggest the use of a simplified, empiric approach for correction of PSMA uptake by applying a specific RoT CF for small lesions according to their size category. This CF could be easily applied clinically when using the PROMISE diagnostic algorithm for small PSMA-avid nodes. Overall, there is good concordance between the miPSMA score obtained using the RoT and the corrected miPSMA score (nearly 90%). Furthermore, the impact of the discordance between miPSMA scores obtained using correction methods versus the RoT on clinical interpretation is likely minor when considering that, for many of these lesions (e.g., nonregional nodes or indeterminate bone lesions on CT), a score of 2 is sufficient for diagnosis of a metastatic deposit and the discordance between a score of 2 and a score of 3 is unlikely to be clinically relevant.

This study had several limitations. First, the patient cohort was a selected population of patients with biochemical failure in whom CT and bone scintigraphy showed negative or equivocal findings. Therefore, these corrections in patients with higher-volume metastatic disease would likely be less clinically relevant. Second, we included only lymph nodes in our analyses. None of the bone lesions that we encountered had a CT correlate; therefore, they could not be segmented accurately for the correction methods used, and none of the patients had proven visceral metastases on PET. It is conceivable that the CF that was identified for nodes may not be applicable to all metastatic sites. Third, the use of 2 different scanners introduces heterogeneity to the data; however, we analyzed the data separately for each scanner according to pixel size. Fourth, the impact of PVC on regional nodal metastases

**TABLE 5**
Corrected Versus RoT $SUV_{max}$ and miPSMA Scores

| | Corrected | | RoT | |
|---|---|---|---|---|
| Lesion size | $SUV_{max}$ | miPSMA | $SUV_{max}$ | miPSMA |
| <4 mm | 21.5 ± 21.2 (5.6–96.3) | 2.1 ± 0.8 | 21.0 ± 20.4 (8.3–101.4), $P = 0.681$ | 2.1 ± 0.6, $P = 0.616$ |
| 4–7 mm | 24.4 ± 19.7 (5.1–116.3) | 2.2 ± 0.8 | 23.7 ± 16.8 (5.1–96.7), $P = 0.184$ | 2.3 ± 0.8, $P = 0.665$ |
| 7–9 mm | 39.0 ± 25.5 (5.8–102.9) | 2.6 ± 0.7 | 37.4 ± 21.0 (8.4–104.5), $P = 0.206$ | 2.6 ± 0.7, $P = 0.905$ |
| 9–12 mm | 39.2 ± 27.1 (8.4–102.0) | 2.5 ± 0.8 | 40.1 ± 28.1 (6.9–103.0), $P = 0.595$ | 2.5 ± 0.8, $P = 0.867$ |

Data are mean ± SD. Numbers in parentheses represent range; range for miPSMA is fixed (1–3) and therefore not included in this table. *P* values are for corrected vs. RoT data.

**TABLE 6**
Distribution of Original, Corrected, and RoT miPSMA Scores

| | Original | | | Corrected | | | RoT | | |
|---|---|---|---|---|---|---|---|---|---|
| Lesion size | Score 1 | Score 2 | Score 3 | Score 1 | Score 2 | Score 3 | Score 1 | Score 2 | Score 3 |
| <4 mm | 20 (91) | 1 (4.5) | 1 (4.5) | 5 (22.7) | 10 (45.5) | 7 (31.8) | 3 (13.6) | 13 (59.1) | 6 (27.3) |
| 4–7 mm | 90 (64.3) | 38 (27.1) | 12 (8.6) | 31 (22.1) | 51 (36.4) | 58 (41.4) | 25 (17.9) | 53 (37.8) | 62 (44.3) |
| 7–9 mm | 15 (30) | 19 (38) | 16 (32) | 6 (12) | 10 (20) | 34 (68) | 5 (10) | 9 (18) | 36 (76) |
| 9–12 mm | 6 (30) | 4 (20) | 10 (50) | 4 (20) | 3 (15) | 13 (65) | 3 (10) | 4 (25) | 13 (65) |

Data are numbers followed by percentages in parentheses.

is unlikely to be clinically relevant, as regional nodes with a score of 1 are considered positive; however, PVC could impact the classification of other deposits such as nonregional nodes. Fifth, we did not have pathology confirmation of PSMA-avid nodes. Finally, this study used a second-generation $^{18}$F-labeled PSMA ligand, and it is uncertain whether these results can be extrapolated to $^{68}$Ga-PSMA tracers or to other $^{18}$F-labeled tracers with a different biodistribution and different background tracer uptake in reference tissues.

## CONCLUSION

A smoothing filter and PVC had a significant effect on measured PSMA activity in small nodal metastases, impacting the miPSMA score. We propose the use of a simplified, clinically applicable RoT CF for tracer uptake in small lesions. The impact of these changes on the management and outcomes of patients with oligometastatic prostate cancer need validation in future clinical studies.

## DISCLOSURE

No potential conflict of interest relevant to this article was reported.

**KEY POINTS**

**QUESTION:** Do partial-volume effect and postprocessing smoothing of images significantly impact the measured PSMA activity in small prostate cancer metastases and the miPSMA score?

**PERTINENT FINDINGS:** In this prospective cohort study, a smoothing filter and PVC had a significant effect on measured PSMA activity in small nodal metastases, impacting the miPSMA score.

**IMPLICATIONS FOR PATIENT CARE:** When PSMA PET images are being evaluated, PVC and smoothing need to be applied for small metastatic lymph nodes.

## REFERENCES


1. Hope TA, Afshar-Oromieh A, Eiberr M, et al. Imaging prostate cancer with PSMA PET/CT and PET/MR: current and future applications. *AJR.* 2018;211:286–294.
2. Werner RA, Derlin R, Lapa C, et al. $^{18}$F-labeled, PSMA-targeted radiotracers: leveraging the advantages of radiofluorination for prostate cancer molecular imaging. *Theranostics.* 2020;10:1–16.
3. Szabo Z, Mena E, Rowe SP, et al. Initial evaluation of [$^{18}$F]DCFPyL for prostate-specific membrane antigen (PSMA)-targeted PET imaging of prostate cancer. *Mol Imaging Biol.* 2015;17:565–574.
4. Eiber M, Herrmann K, Calais J, et al. Prostate Cancer Molecular Imaging Standardized Evaluation (PROMISE): proposed miTNM classification for the interpretation of PSMA-ligand PET/CT. *J Nucl Med.* 2018;59:469–478.
5. Soret M, Bacharach SL, Buvat I, et al. Partial-volume effect in PET tumor imaging. *J Nucl Med.* 2007;48:932–945.
6. Boussion N, Cheze Le Rest C, Hatt M, et al. Incorporation of wavelet-based denoising in iterative deconvolution for partial volume correction in whole-body PET imaging. *Eur J Nucl Med Mol Imaging.* 2009;36:1064–1075.
7. Cysouw MCF, Kramer GM, Schoonmade LJ, et al. Impact of partial-volume correction in oncological PET studies: a systematic review and meta-analysis. *Eur J Nucl Med Mol Imaging.* 2017;44:2105–2116.
8. Ravert HT, Holt DP, Chen Y, et al. An improved synthesis of the radiolabeled prostate-specific membrane antigen inhibitor, [$^{18}$F]DCFPyL. *J Labelled Comp Radiopharm.* 2016;59:439–450.
9. Biehl KJ, Dehdashti F, Feng Ming K, et al. $^{18}$F-FDG PET definition of gross tumor volume for radiotherapy of non-small cell lung cancer: is a single standardized uptake value threshold approach appropriate? *J Nucl Med.* 2006;47:1808–1812.
10. Lucy LB. An iteration technique for the rectification of observed distributions. *Astron J.* 1974;79:745–754.
11. Richardson WH. Bayesian-based iterative method of image restoration. *J Opt Soc Am.* 1972;62:55–59.
12. Ost P, Reynders D, Decaestecker K, et al. Surveillance or metastases-directed therapy for oligometastatic prostate cancer recurrence: a prospective, randomized, multicenter phase II trial. *J Clin Oncol.* 2018;36:446–453.
13. Tosoian JJ, Gorin MA, Ross AE, et al. Oligometastatic prostate cancer: definitions, clinical outcomes, and treatment considerations. *Nat Rev Urol.* 2017;14:15–25.
14. Kneebone A, Hruby G, Ainsworth H, et al. Stereotactic body radiotherapy for oligometastatic prostate cancer detected via prostate-specific membrane antigen positron emission tomography. *Eur Urol Oncol.* 2018;1:531–537.
15. Wright CL, Binzel K, Zhang J, Knopp MV. Advanced functional tumor imaging and precision nuclear medicine enabled by digital PET technologies. *Contrast Media Mol Imaging.* 2017;2017:5260305.